Journal of Fluids and Structures (2000) **14,** 883–893
doi:10.1006/jfls.2000.0298, available online at http://www.idealibrary.com on IDEAL®

GLOBAL CHAOS IN FLOW-INDUCED OSCILLATIONS OF CYLINDERS

P. Plaschko

Universidad Autónoma Metropolitana
Iztapalapa, 09340 México D.F., México

(Received 3 December 1998, and in final form 21 February 2000)

Flow-induced cylinder vibrations can be approximately described by the dynamics of a Hamiltonian system excited at a fundamental and a higher harmonic frequency. Three resonances arise and each of them is associated with a heteroclinic path. The overlap of a pair of tori yields global chaos, the onset of which is calculated with the Chirikov method. An averaging approximation is used and a comparison with the exact solution shows excellent agreement in the low-energy limit. The transition occurs along a locus curve which relates the wind speed to the frequency parameter. Poincaré maps confirm qualitatively the theoretical predicted transition.

1. INTRODUCTION

A SEMI-EMPIRICAL MODEL governing flow-induced vibrations of cylinders was developed and discussed in previous papers (Berger 1988; Berger & Plaschko 1993). A multiple-scales approach is used to show that the flow oscillations can be described with inhomogeneous equations decoupled from the rest of the system (Plaschko 1996). The excitations of the flow is caused by the fundamental and higher harmonic oscillations of the cylinder. This simplified system (with the excitation as a small perturbation) was tackled with the Melnikov method and a break-up of heteroclinic orbits of the unperturbed system was found. This break-up occurs in a sub-space of parameters and it leads to local chaos near the unperturbed heteroclinic orbit.

In the present paper, we go a step beyond this. We study weakly damped flow oscillations and show that three nonlinear resonances exist. This individual resonances are associated with heteroclinic orbits which can be considered as resonance bands. As the perturbation parameter is raised, the width of these bands grows and they may finally overlap to form large-band global chaos. We apply the overlap criterion (Chirikov 1979) to predict the onset of this global chaos. The Chirikov method uses an averaging approximation which leads, generally, only to a correct prediction of the order of magnitude of the parameters governing the transition (Lin & Reichel 1986). We will show, however, that the averaging yields, in the low-energy limit, results which correctly approximate the exact solutions. We will discuss in Appendix A the problems which arise if alternative techniques, like the elliptic-function approach or the renormalization procedure (Escande 1985), are used.

2. ANALYSIS

It is well known that dissipative effects leads to limit-cycle cylinder motions. Berger's (1988) nonlinear model has been successfully used to describe such periodic cylinder oscillations

0889–9746/00/080883 + 11 $35.00/0

(Berger & Plaschko, 1993). Moreover, this model has the power to predict hysteresis, as found in experiments [cylinder in air: Feng (1968) and Kobayashi (1980); flexing cylinder in air: Brika & Laneville (1993); cylinder in water: Khalak & Williamson (1996)]. To compare our theoretical predictions with experimental findings, see, e.g. figure 6 in Berger & Plaschko and figure 9 in Brika & Laneville.

In the present paper we focus, however, exclusively on fluid dynamical oscillations and not on the motion of the cylinder itself. It has been shown previously that, in the case of very low values of the mass ratio, the evolution of the lift coefficient can be separated from the equation that dominates the cylinder oscillations. The flow is characterized by the lift coefficient and we study the temporal evolution of the lift. The periodic cylinder oscillation manifests itself in terms of a feedback which represents an inhomogeneity in the lift equation.

We refrain from giving a detailed account of the model equations and we refer the reader to the derivation given by Berger & Plaschko (1993). The decoupling of the flow equations was discussed by Plaschko [1996; equation (4)]. This yields an equation governing the lift coefficient $x(t)$ excited by the cylinder oscillations

$$\ddot{x} + (\xi_0 + \xi_2 \dot{x}^2)\dot{x} + (\Omega^2 - \beta^2 x^2)\, x = a_1 \cos(t) + a_3 \cos(3t), \tag{1}$$

where t is the time and dots denote time derivatives; $\xi_0 < 0$ and $\xi_2 > 0$ are damping coefficients, $\Omega > 1$ is the wind speed, and β is a frequency constant. The right-hand side of equation (1) is caused by the oscillations of the cylinder which, for small values of the mass ratio n (i.e. the ratio of the mass of the fluid displaced by the cylinder, to the mass of the cylinder), oscillates at unit frequency and with the amplitude A given by

$$A^2 = \frac{4}{3}\frac{d_0\Omega_1 - n_1 b_0}{n_1 b_2 - d_2\Omega_1}, \quad \Omega_1 = \Omega^2 - 1, \quad n_1 = nU^2. \tag{2}$$

The cylinder damping constants and feedback coefficients $d_{0,2}$ and $b_{0,2}$, appearing in equation (2) are given by

$$d_0 = D_{0f} + n\Omega_1 D_{1f}, \quad d_2 = 4n\Omega_1 D_{2f},$$
$$b_0 = \Omega_1 B_{0f}, \quad b_2 = 4\Omega_1 B_{2f}, \tag{3}$$

with the constants D_{0f}, D_{2f} and B_{0f}, B_{2f} being determined by fits to experimental data (Kobayashi 1980) and listed in Appendix B. We mention here only the relation $B_{0f} > 0$ and $B_{2f} < 0$. The amplitudes $a_{1,3}$ have the form

$$a_1 = (b_0 + \tfrac{3}{4} b_2 A^2)A, \quad a_3 = \tfrac{1}{4} b_2 A^3. \tag{4}$$

It could be argued that it is easy to solve (1) numerically and to study in this way the onset of (global) chaos. Such an *a priori* numerical approach would, however, involve the somewhat awesome consideration of a system in a rather high-dimensional parameter space. In contrast, we base the following investigation on an approximate analysis and we shall compare the prediction thus derived with the results obtained from numerically calculated Poincaré maps.

The study of the transition to global chaos will be based on the following scaling:

$$\xi_0, \xi_2 = \mathcal{O}(\varepsilon^2), \quad D_{0f} = q_0\varepsilon, \quad n = n_0\varepsilon, \quad \Omega = 1 + \omega\varepsilon/2, \quad \varepsilon \to 0_+, \tag{5}$$

where the coefficients are order-one constants. The Ω-scaling is motivated by experimental work of, amongst others, Brika & Laneville (1993) and Khalak & Williamson (1996). These experiments indicate harmonic cylinder motions in a narrow band located at about

$0{\cdot}9 \leq \Omega \leq 1{\cdot}2$. This synchronization interval is well predicted by the numerical results ($1{\cdot}005 \leq \Omega \leq 1{\cdot}225$) presented by Berger & Plaschko (1993). The fluid motion—as characterized by the lift coefficient—is, however, much less regular than the harmonic cylinder oscillations (see the temporal evolution and spectral measurements revealed in figures 6 and 7 of Khalak & Williamson). Note also that the latter experiments have been performed for moderately high values of the Reynolds number ($\mathrm{Re} = 10\,600$). Our present study concentrates, however, on nearly undamped fluid oscillations, see equation (5), and this corresponds to higher values of the Reynolds number and thus to more irregular flows. Previous numerical results (Plaschko 1996) give evidence that these irregular flow oscillations take place also at wind speeds near $\Omega = 1$. Thus, we obtain from equations (2) and (5)

$$A^2 = \frac{4}{3}\frac{n_0\lambda_0 U_1^2 - q_0}{n_0 U_1^2|\lambda_2|} = \mathcal{O}(1),$$

$$U_1 = U(0); \quad \lambda_0 = B_{0f} > 0, \quad \lambda_2 = 4B_{2f} < 0. \tag{6}$$

The oscillator is governed by

$$\ddot{x} + (1 - \beta^2 x^2)x = \varepsilon\omega\,[\alpha_1 \cos(t) + \alpha_3 \cos(3t) - x] + \mathcal{O}(\varepsilon^2), \tag{7}$$

with

$$\alpha_1 = \left(\lambda_0 + \frac{3}{4}\lambda_2 A^2\right)A > 0, \quad \alpha_3 = \frac{1}{4}\lambda_2 A^3 < 0. \tag{8}$$

It is now easy to see that the oscillator equation (7) is equivalent to the canonical equations of the Hamiltonian ($\mathcal{O}(\varepsilon^2)$-terms are suppressed from now on)

$$H = H_0 + \varepsilon H_1 + \mathcal{O}(\varepsilon^2), \tag{9}$$

with

$$H_0 = \frac{1}{2}(q^2 + p^2) - \frac{\beta^2}{4}q^4; \quad q = x; \quad p = \dot{x};$$

$$H_1 = -\omega\{q[\alpha_1 \cos(t) + \alpha_3 \cos(3t)] - q^2/2\}. \tag{10}$$

Note that the unperturbed problem exhibits a centre in the origin and two saddles at $(q, p) = (\pm 1/\beta, 0)$. The hyperbolic points are associated with a heteroclinic orbit which is (for $0 < E_0 < 1/(4\beta^2)$) filled with periodic paths surrounding the origin.

There are two alternative strategies to study the onset of global chaos: (a) the elliptic function approach and (b) the averaging approximation, which will be discussed in what follows.

2.1. Elliptic Function Approach

This precise method is to define action-angle variables, transform the Hamiltonian (10) with these variables, and pass on to the study the possibility of overlapping tori. Here, we start from the unperturbed part of equation (10), with energy E_0. We solve this for p and obtain

$$p = \pm\frac{\beta}{\sqrt{2}}\sqrt{(u_+ - q^2)(u_- - q^2)}, \quad u_\pm = \frac{1 \pm \sqrt{1 - 4E_0\beta^2}}{\beta^2},$$

with

$$u_+ \to 2(1 - E_0\beta^2)/\beta^2, \quad u_- \to 2E_0 \quad \text{for } E_0 \to 0. \tag{11}$$

Next, we use the standard definition of the action variable I (Goldstein 1980),

$$I = \frac{1}{2\pi} \int p \, \mathrm{d}q,$$

where the integral denotes the integration over a period. To find the period we note that, in the regime of periodic motions $|q| < 1/\beta$, the potential $V = (1/2)\,(q^2 - \beta^2\, q^4/2)$ and hence the energy is positive. Thus, from equation (11) we obtain $0 < E_0 < 1/(4\beta^2)$ and $u_+ > 1/\beta^2$, $u_- < 1/\beta^2$. We have to consider to zeros of p for $q = \pm\sqrt{u_-}$, therefore. This gives the action variable the form

$$I = \frac{\beta\sqrt{2}}{\pi} \int_0^{\sqrt{u_-}} [(u_+ - q^2)(u_- - q^2)]^{1/2} \, \mathrm{d}q. \tag{12}$$

It is easy to derive from equation (12) that

$$I = E_0 + \mathcal{O}(E_0^2) \tag{12a}$$

Next, we want to calculate the frequency defined by

$$\nu = (E_0, \beta) = \frac{\partial E_0}{\partial I} \tag{13}$$

and we use equation (12) to calculate the inverse frequency. Thus we obtain [see, e.g. Lawden (1989)]

$$\frac{1}{\nu} = \frac{2\sqrt{2}}{\beta\pi} \int_0^{\sqrt{u_-}} [(u_+ - q^2)(u_- - q^2)]^{1/2} \, \mathrm{d}q$$

$$= \frac{2}{\beta\pi} (2/u_+)^{1/2} \, \mathrm{K}(k), \quad k^2 = u_-/u_+, \tag{14}$$

where $\mathrm{K}(k) = \pi(1 + k^2/4 + \mathcal{O}(k^4))/2$ denotes the complete elliptic integral of the first kind and k is its modulus. We expand equation (14) for small energies and this yields

$$\nu = 1 - \frac{3}{4}\,\beta^2\, E_0 + \mathcal{O}(E_0^2). \tag{14a}$$

We do not continue for the moment to use this "heavy machinery" of elliptic functions and we shall return to this exact approach in Appendix A. In the following, we approximate the unperturbed Hamiltonian by its average value. We shall compare the frequency obtained with this approximation to the frequency calculated with the exact analysis using equations (12) and (13).

2.2. Averaging Approximation

Here we use the canonical transform

$$q = \sqrt{2J} \sin \Theta, \quad p = \sqrt{2J} \cos \Theta, \tag{15}$$

where (J, Θ) are modified (or approximated) action-angle variables. Hence, we obtain from equation (10) the unperturbed "new" Hamiltonian

$$R_0 = J - J^2\, \beta^2 \sin^4 \Theta. \tag{16}$$

Now, we average equation (16) and obtain

$$\bar{R}_0 = \frac{1}{2\pi}\int_0^{2\pi} R_0(\Theta, J)\,\mathrm{d}\Theta = J - 3J^2\beta^2/8. \tag{17}$$

To get an error estimate we compare the frequency of the averaged system

$$\bar{\nu} = \left.\frac{\partial R_0}{\partial J}\right|_{J=1} = 1 - 3I\,\beta^2/4, \tag{18}$$

with the frequency in equation (14a). We see that the first two terms of the expansion (14a) agree with (18) where l is substituted from equation (12a). The result of the numerical evaluation of equation (14) is shown in Figure 1 and again compared with equation (18). From this we see that the agreement of the two frequencies is striking in the low-energy range. Only in a region near the saddles ($E_0 = 4/\beta^2$) there appears a slight deviation.

Next, we apply transform (16) also to the perturbed part of equation (10) and we obtain

$$R = \bar{R}_0 + \varepsilon R_1,$$

$$R_1 = -\frac{\omega}{2}((2J)^{1/2}\{\alpha_1[\sin(\Theta - t) + \sin(\Theta + t)] \tag{19}$$

$$+ \alpha_3[\sin(\Theta - 3t) + \sin(\Theta + 3t)]\} - 2J\sin^2\Theta).$$

Note that there appear five types of excitation waves in equation (19) with wave velocities $\dot{\Theta}_w = 0,\ \pm 1,\ \pm 3$. The nonlinearity of system (19) causes primary resonances, with the resonance condition [see, e.g. Reichel (1992)]

$$\bar{\omega} = 1 - 3\beta^2 J/4 = \dot{\Theta}_w. \tag{20}$$

Thus, we obtain three individual primary resonances located at

$$J = a,\ 2a,\ 4a, \quad a = 4/(3\beta^2) \tag{21}$$

and in all three cases we face a nonremovable term in R_1. Note the location of resonances (21) could be also derived with the use of a perturbation expansion such as Lie transforms [see, e.g. Lichtenberg & Liebermann (1983)].

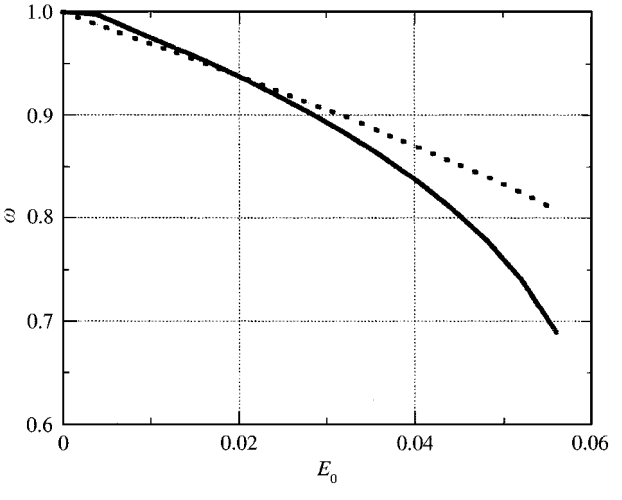

FIGURE 1. Comparison of averaged (dotted line) and exact (continuous line) frequencies; $\beta = 2$.

It is now convenient to express the nonautonomous system (19) as an extended autonomous one. We use $Q = t$ and P as the additional pair of action-angle variables and we obtain

$$Z = Z_0 + \varepsilon Z_1, \quad Z_0 = \bar{R}_0 + P,$$

$$Z_1 = -\frac{\omega}{2}((2J)^{1/2}\{[\alpha_1 \sin(\Theta - Q) + \sin(\Theta + Q)] + \alpha_3[\sin(\Theta - 3Q) + \sin(\Theta + 3Q)]\} - 2J\sin^2\Theta). \tag{22}$$

In the following, we investigate the three resonances separately and we will find that each resonance is associated with a heteroclinic path or torus. If the expansion parameter grows the tori may approach each other and this leads to daughter resonates and hence to global chaos. We consider in the following each resonance separately. We will investigate the location and the size of each resonance band then use the Chirikov overlap criterion to calculate the value of ε for the onset of global chaos.

2.2.1. *The resonance for $j = a$*

Here we obtain from equation (22) the Hamiltonian

$$Z = J - 3(J\beta)^2/8 + P + \omega\varepsilon J\sin^2\Theta, \tag{23}$$

Q is a cyclic variable cyclic variable and we have $P = \text{const}$. We can disregard the latter variable and we obtain an autonomous one-degree-of-freedom (1-dof) system. Its fixed points are in leading order:

$$(\Theta, J) = (0, a), (\pm\pi, a) \quad \text{hyperbolic points},$$
$$(\Theta, J) = (\pm\pi/2, a) \quad \text{elliptic points}. \tag{24}$$

The heteroclinic path corresponding to this resonance is given by

$$T_1 : Z(J, \Theta) = Z(a, 0).$$

It connects the hyperbolic points to each other and its maximal height (which occurs at $\Theta = \pm\pi/2$) is given as

$$J_{1\max} = a(1 \pm \sqrt{2\varepsilon\omega} + \varepsilon\omega) + \mathcal{O}((\varepsilon\omega)^{3/2}). \tag{25}$$

2.2.2. *The resonance for $J = 2a, 4a$*

The Hamiltonian is now given by

$$Z = J - 3(J\beta)^2/8 + P - \omega\varepsilon\alpha_j\sqrt{\frac{J}{2}}\sin(\Theta + f_jQ), \quad f_1 = 1, f_3 = 3. \tag{26}$$

We introduce the canonical transform

$$U = \Theta + f_jQ, \quad V = J, \quad U_2 = Q, \quad V_2 = P - f_jV. \tag{27}$$

Substitution into equation (26) yields

$$\hat{Z} = (1 + f_j)V - 3(V\beta)^2/8 + V_2 - \omega\varepsilon\alpha_j\sqrt{\frac{V}{2}}\sin(U).$$

Therefore, the variable U_2 is cyclic and V_2 is constant. Thus, we obtain again an $1-$ dof Hamiltonian,

$$\tilde{Z} = (1+f_j)\,V - 3(V\beta)^2/8 - \omega\varepsilon\alpha_j\sqrt{\frac{V}{2}}\sin(U). \tag{28}$$

Taking into account that $\alpha_1 > 0, \alpha_3 < 0$, we find the fixed points to be located at

$$J = 2a: \begin{cases}(U, V) = (\pi/2, b_1), (-3\pi/2, b_1) & \text{hyperbolic points,}\\ (U, V) = (-\pi/2, b_1), (-3\pi/2, b_1) & \text{elliptic points}\end{cases} \tag{29}$$

and

$$J = 4a: \begin{cases}(U, V) = (-\pi/2, b_3), (3\pi/2, b_3) & \text{hyperbolic points,}\\ (U, V) = (\pi/2, b_3), (-3\pi/2, b_3) & \text{elliptic points.}\end{cases} \tag{30}$$

Equation (28) admits solutions which are 2π-periodic with respect to the variable U. In equation (29) and (30) we list, however, only the location of the fundamental fixed points. $b_{1,3}$, the V-coordinates of the hyperbolic points, are obtained as the solution of the bicubic equation

$$\sigma^3 + w\sigma + \varepsilon\tilde{q} = 0, \quad b_{1,3} = \sigma^2,$$
$$w = -a(1+f_j), \quad \tilde{q} = 2^{1/2}\omega|\alpha_j|/(3\beta^2). \tag{31}$$

Note that this cubic equation has three real roots. We use an expansion to solve equation (31) and we obtain

$$b_j = |w| \pm \varepsilon q/\sqrt{|w|}, \tag{32}$$

and we suppress the trivial solution for bs. The corresponding tori are thus given by

$$T_1: Z(U, V) = Z(\pi/2, b_1), \quad T_3: Z(U, V) = Z(-\pi/2, b_3).$$

An expansion fails, however, to calculate the maximal heights (located for $J = 2\,a(J = 4a)$ at $U = -\pi/2(U = \pi/2)$.) and we have to calculate these quantities numerically. Note that the tori $J = a$ and $J = 2a$ exhibit at $U = \Theta = -\pi/2$ a common position of maximal elongation in the $J-$ direction.

3. NUMERICAL RESULTS

Now we can investigate the overlap of the individual tori. We used exclusively the parameters

$$q_0 = n_0 = 1 \tag{33}$$

and varied β, ε and ω. The two latter parameters appear, however, only in the combination $\varepsilon\omega = 2(\Omega - 1)$.

It turns out that the only overlap which allows small expansion parameters occurs between the tori $J = a$ and $J = 2a$. The corresponding numerical findings are revealed in Figure 2. The locus of the onset of global chaos is plotted in this figure. The globally chaotic region lies above this curve, and we restricted the values of β such that the term proportional to β^2 in equation (11) is not singular. This figure shows that the onset of global chaos takes place for values of the perturbation parameter (the deviation of the wind speed from unity) which still are small enough to justify the omission of higher-order terms.

Poincaré maps (snapshots taken at integer multiples of 2π) are calculated to determine the onset of global chaos numerically. For comparatively small values of $\varepsilon\omega$ this map has

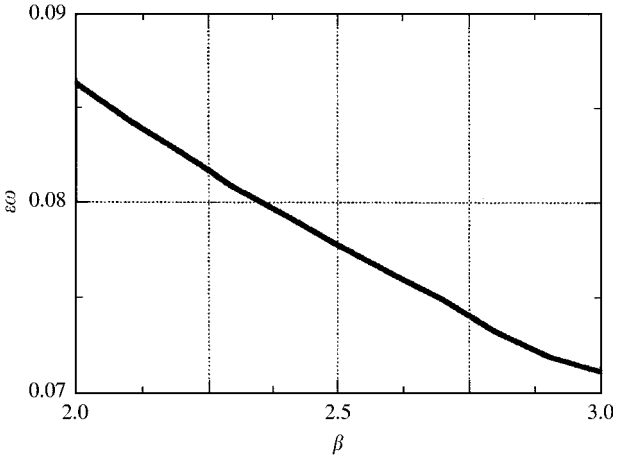

FIGURE 2. Locus of the transition to global chaos, $\omega = 1$.

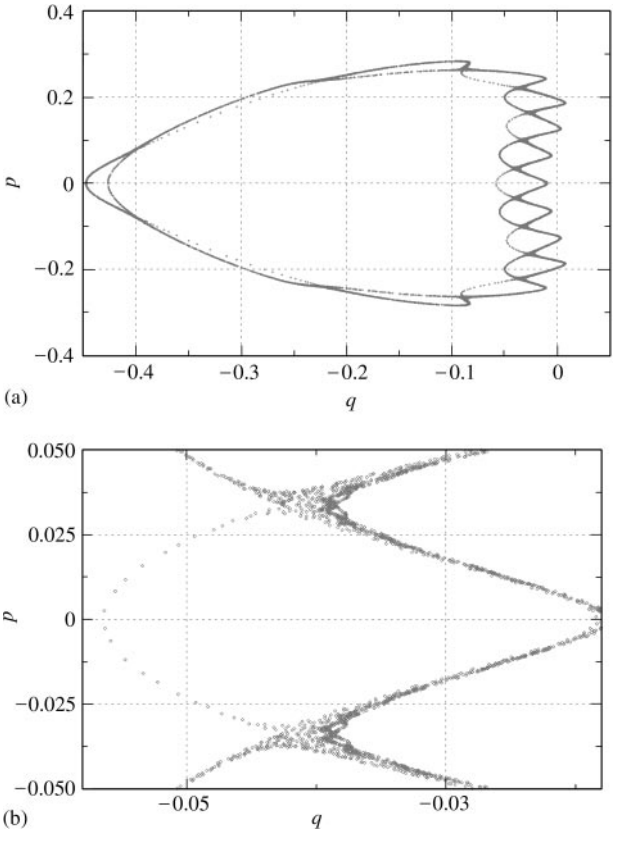

FIGURE 3(a, b). Poincaré sections of the oscillator of equation (7) taken at $t = 2n\pi$, $\beta = 2$, $\omega = 1$, $\varepsilon = 0{\cdot}0875$, with initial conditions $q(0) = -0{\cdot}01$, $p(0) = 0$. Figure 3(b) is a blow up of Figure 3(a). The plot corresponds to a single trajectory followed for 18 000 periods.

the form of a closed curve, which confirms the existence of a torus in the (q, p, t)-space. An increase of $\varepsilon\omega$ leads first to the development of a wavy structure. The latter occurs in a $(q\text{-}p)$-diagram at the right margin of the map. This structure persists for $\varepsilon\omega < 0{\cdot}085$.

A particular Poincaré map is shown in Figure 3(a, b) for the slightly higher value $\varepsilon\omega = 0{\cdot}0875$. There appear two intersecting wavy structures at the right margin of this map [Figure 3(a)]. A blow up [Figure 3(b)] shows a scatter of points near the intersections and thus indicates the transition to global chaos.

Our predictions pertain to almost undamped (and hence high Reynolds number) fluid oscillations. Experimental data of lift oscillations published so far focus, however, only on intermediately high values of the Reynolds number. To perform a comparison with the experimental findings of Khalak & Williamson we present now in Figures 4 and 5 the temporal evolution of the lift coefficient $q(t)$ and its power spectrum, respectively. The maximal amplitude of the lift oscillation has according to Figure 4 a value of about 0·4. The latter value is in agreement with the observations of oscillation amplitudes in the lower Reynolds number regime, see figure 6 in Khalak & Williamson (1996). The almost undamped oscillations are, however, predicted to vary much more irregularly than the observed

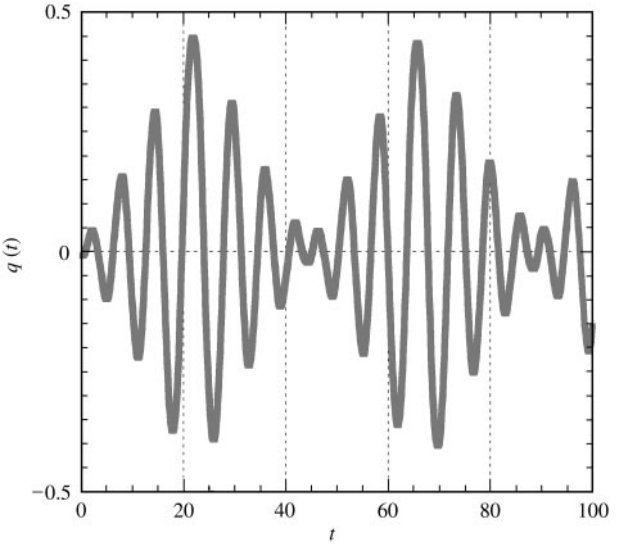

FIGURE 4. Temporal evolution of the lift coefficient $q(t)$, for parameters as in Figure 3.

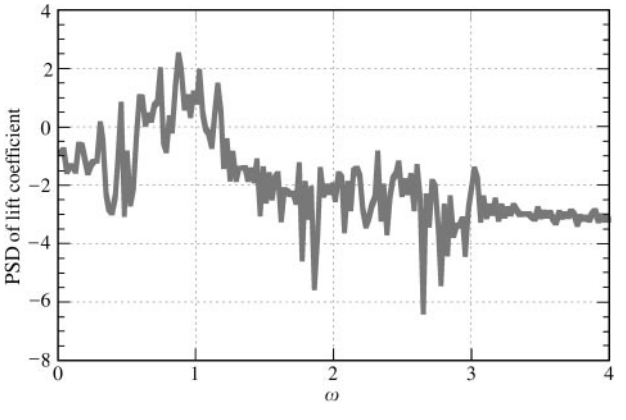

FIGURE 5. Power spectrum of the lift coefficient; parameters as in Figure 3. The frequency parameter $\omega = 2\pi f$ in this plot should not be confused with the wind speed parameter ω defined in the last part of equation of (5).

lower Reynolds number oscillations. This can be seen from a comparison of our noisy power spectrum (Figure 5) with the corresponding experimental data (figure 7 in Khalak & Williamson). The dominant peak of our spectrum lies at about $\omega = 2\pi f = 1$, which is close to the experimental value of about $f = 0{\cdot}23$ (with a decreasing tendency as Re grows) in figure 8 Khalak & Williamson.

4. CONCLUDING REMARKS

An interesting generalization of the present study would be the inclusion of stochastic noise. Helpful hints to perform such an analysis are given in the recent literature (Øksendal 1998). We hope we shall return in the near future to tackle this challenging problem. We consider also performing an experimental study of cylinder vibrations. Previous funding has been foiled, however, by the Mexican Peso-crisis. We hope that we shall soon be able to finance a test-section, such that we can start experimental studies to support the theoretical predictions.

References

Berger, E. 1988 On a mechanism of vortex excited oscillations of a cylinder. *Journal of Wind Engineering and Industrial Aerodynamics* **28,** 301–319.

Berger, E. & Plaschko, P. 1993 Hopf bifurcations and hysteresis in flow-induced vibrations of cylinders. *Journal of Fluid and Structures* **7,** 849–866.

Brika, D. & Laneville, A. 1993 Vortex-induced vibrations of a long flexible circular cylinder. *Journal of Fluid Mechanics* **250,** 481–508.

Chirikov, B. V. 1979 Universal instability of many-dimension oscillatory systems. *Physics Reports* **52,** 263–279.

Escande, D. F. 1985 Stochasticity in classical Hamiltonian systems: Universal aspects. *Physics Reports* **121,** 165–172.

Feng, C. C. 1968 The measurement of vortex induced effects in flow past stationary and oscillating circular and D-section cylinders. Master's thesis, University British Columbia, Vancouver, B.C., Canada.

Goldstein, H. 1980 *Classical Mechanics.* Reading, MA: Addison-Wesley.

Khalak, A. & Williamson, C. H. K. 1996 Dynamics of a hydroelastic cylinder with very low mass and damping. *Journal of Fluid and Structures* **10,** 455–472.

Kobayashi, T. 1980 Schwingungen von federgelagerten, stumpfen Zylindern infolge Wirbelalösung. Dissertation, Technical University of Berlin, D 83, FB 9, Berlin, Germany (in German).

Lawden, D. F. 1989 *Elliptic Functions and Applications.* New York: Springer-Verlag.

Liebermann, M. A. & Lichtenberg, A. J. 1983 *Regular and Stochastic Motion.* New York: Springer-Verlag.

Lin, W. A. & Reichel, L. E. 1986 External field induced chaos in an infinite square well potential. *Physica* **19**D, 145–152.

Øksendal, B. 1998 *Stochastic Differential Equations*: *An Introduction.* New York: Springer-Verlag.

Plaschko, P. 1996 Heteroclinic bifurcations in flow-induced oscillations of cylinders. *Journal of Fluids and Structures* **10,** 33–46.

Reichel, L. E. 1992 *The Transition to Chaos.* New York: Springer-Verlag.

APPENDIX A

It is easy to show that the exact solution of the unperturbed part of equation (7) is given by

$$x(t) = B\,\mathrm{sn}(ft, k), \quad k = \sqrt{1/f^2 - 1}, \quad B = \sqrt{2(1-f^2)}/\beta, \quad 0 < f < 1, \tag{A1}$$

where sn denotes the Jacobi elliptic function. With this we obtain from equation (10) the unperturbed Hamiltonian

$$E_0 = (1 - f^2) f^2/\beta^2. \tag{A2}$$

To establish an appropriate action-angle transform we recall the periodicity $4\,\mathrm{K}(k)$ of the sn-function. Thus, we define the angle variable Θ which varies from 0 to 2π as

$$x(t) = B\,\mathrm{sn}(\lambda), \quad \lambda = (2K\,\Theta/\pi, k), \quad \text{or } \dot{\Theta} = \frac{f\pi}{2K}. \tag{A3}$$

The action variable is obtained if we observe the definition

$$\dot{\Theta} = E_{0I} = E_{0f} f_I.$$

Thus, after an integration, we derive from equations (A2) and (A3)

$$I = \frac{4K}{\pi\beta^2}\left(f - \frac{2}{3}f^3\right) + \text{const.} \tag{A4}$$

We solve equation (A2) for f and we obtain

$$f_{1,2}^2 = \frac{1}{2}[1 \pm (1 - 4E_0\beta^2)^{1/2}] = u_{\pm}\beta^2/2. \tag{A5}$$

The modulus of elliptic functions is restricted to $0 < k < 1$. Because of the second part of equation (A1) we must choose $\frac{1}{2} \le f^2 \le 1$ and, considering again the low-energy limit, we have to take the plus sign in equation (A5). This yields

$$f^2 = 1 - E_0\beta^2, \qquad k = \beta\sqrt{E_0}, \quad B = \sqrt{2E_0} \quad \text{for } E_0 \to 0. \tag{A6}$$

We introduce now the canonical transform (A3) with $q = x(t)$, $p = \dot{x}(t)$ into equation (10) and this yields

$$H_1 = -\omega\{B\,\mathrm{sn}(\lambda)[\alpha_1\cos(t) + \alpha_3\cos(3t)] - B^2\,\mathrm{sn}^2(\lambda)/2\}. \tag{A7}$$

The Fourier decomposition of the sn-function is given by

$$\mathrm{sn}(\lambda) = \frac{2\pi\sqrt{e}}{kK}\left[\frac{\sin\Theta}{1-e} + \frac{e\sin(3\Theta)}{1-e^3} + \mathcal{O}(e^2)\right]; \tag{A8}$$

$e = e(f)$ denotes the nome of the elliptic functions and it has for small values of the modulus the expansion $e \to k^2/16 + \mathcal{O}(k^4)$ for $k \to 0$. Thus, we obtain from equation (A8)

$$\mathrm{sn}(\lambda) = \sin\Theta + \frac{\beta^2 E_0}{4}\sin^3(\Theta) + \mathcal{O}(E_0^2). \tag{A9}$$

Equation (A9) and the third part of (A6) lead together with equation (12a) to the low-energy limit $x = \sqrt{2I}\sin\Theta$ and this again to equation (15). Thus, we see that the averaging procedure and the use of the "action-angle variable" (15) represent the lowest order approximation to the exact solutions and transformations.

Finally, we mention the renormalization routine developed to predict onset of global chaos (Escande 1985) and employed later in a number of simple examples (Reichel 1992). This approach applies, however, only to the rather restricted class of Hamiltonian systems

$$H = \frac{p^2}{2} + a_0\cos(x) + a_1\cos[\omega(x - t)]$$

and we cannot use this method to tackle our problem.

APPENDIX B

Here, we list the fit constants which appear in equation (3). Firstly, the resonance speed at unit wind speed $U_1 = U(\Omega = 1)$ has the value $U_1 = 0{\cdot}792708$. With this we obtain

$$B_{0f} = 3{\cdot}223668/U_1^2, \quad B_{2f} = -17{\cdot}79084/(3U_1^4),$$
$$D_{1f} = 2{\cdot}416253/U_1^2, \quad D_{2f} = -14{\cdot}629367/(3U_1^4).$$

Note also that the constant D_{0f} is defined in equation (5).